International Journal of Solids and Structures 51 (2014) 3439–3448

Contents lists available at ScienceDirect

International Journal of Solids and Structures

journal homepage: www.elsevier.com/locate/ijsolstr

Confirming Inextensional Theory

V.R. Seereeram, K.A. Seffen *

Department of Engineering, University of Cambridge, Trumpington Street, Cambridge CB2 1PZ, United Kingdom

ARTICLE INFO

Article history:
Received 28 March 2014
Received in revised form 7 May 2014
Available online 24 June 2014

Keywords:
Inextensional
Thin plates
Developable
Theory
Experiments
Finite element analysis

ABSTRACT

Thin, initially-flat plates can deform inextensionally and elastically during large out-of-plane deformations. This paper revisits an analytical method for describing the developable shapes of displaced plate, in order to quantify and validate its effectiveness. Results from practical experiments and finite element analysis are compared to theoretical predictions from well-known examples, and excellent correlations are obtained.

1. Introduction

Inextensional Theory was developed by Mansfield (1955) nearly 60 years ago for predicting the large-displacement, elastic shape of transversely-loaded, thin-walled elastic plates, typically used in aircraft structures. Shallow, or small, displacement methods are inadequate because they do not deal with the in-plane, or membrane, stresses concomitant to the build-up of moderate deflections—even those of the order of the thickness of the plate. Under larger deflections, Mansfield argues that, for simply-held plates, these membrane stresses and hence, strains are eventually curtailed because significant in-plane forces cannot be transmitted from the supporting boundary of the plate into the bulk of the structure. In the limit, he assumes that the membrane strains are zero, which permits a simplification of the deformed shape of plate in obeyance to Gauss's *Theorema Egregium*, namely, that it becomes a *developable* surface.

Mansfield renders the surface relative to the initial flat state as a general conical displacement field, and then using calculus of variations, the spatial distribution of corresponding conical *generators* is found by maximising the strain energy stored in plate under load, leading to a governing differential equation of generator layout. The variational nature of this formulation with its requirement of general, non-parallel generators was first proposed by Maxwell almost a century before (Niven, 1890) but without a generalised framework for its solution, as delivered by Mansfield. Some years later, Mansfield recognises that his theory is analogous to the earlier Tension Field Theory of Wagner for computing the shape of wrinkled regions in thin-walled terrestrial structures mainly under in-plane shear loads. Consequently, parallels between both types of problem and their performances emerge, for example, a higher theoretical stiffness is predicted because the displacement field is prescribed in both.

Mansfield provides insightful solutions for a few of his cases, including tip-loaded cantilevers and end-loaded strips as idealised models of aircraft wings, where he focusses mainly on calculating the load–deflection responses. In the case of a triangular plate, he also extracts a rudimentary picture of the generator layout using a strain lacquer painted onto the surface, which cracks in the direction of principal tensile strains after loading (Mansfield and Kleeman, 1955). Theoretical predictions of generators successfully compare when they are overlaid in this picture and, importantly, the experiment also confirms that the layout is fixed only by the loading type and planform geometry, and not by the loading magnitude, when displacements are greater than the thickness of plate. In other cases, the layout is not confirmed directly by experiment; instead Mansfield exploits the analogy with Tension Field Theory by devising wrinkled specimens of the same geometrical proportions and equivalent boundary conditions, where the highly visible outline of crests and troughs normal to wrinkles gives equivalent information on the expected layout of generators in his bending experiments: see Mansfield (1989).

The properties of generators may be gleaned instead from the displacement field of the plate, which is then transformed into generator data. For accuracy and completeness, it is necessary to

* Corresponding author. Tel.: +44 1223 764137.
E-mail address: kas14@cam.ac.uk (K.A. Seffen).

http://dx.doi.org/10.1016/j.ijsolstr.2014.06.001
0020-7683/

obtain a highly-resolved, three-dimensional map of the entire deformed surface, and this is now possible with recent advances in photographic technology that we describe later. Therefore, one aim of this study is to validate Inextensional Theory directly at a displacement level by comparing predictions of conical generators with those computed from the measured data: this quantitative comparison is absent from the literature but we are mindful that it achieves same visual objective as Mansfield's single experiment with lacquer. In doing so, we underline the value of Inextensional Theory but we also aim to widen its appeal to other researchers in view of a recent resurgence in problems featuring developable plates and shells, beyond Mansfield's cantilever plates. For example, the large deformation of confined shells provides some insight into the quantum world of dislocation movement in materials (Cerda and Mahadevan, 2005) and into the efficient storage of DNA ribbons within cells (Giomi and Mahadevan, 2010); macroscopically, the random crumpling of paper can be described by developable regions interconnected by sharp ridges (Amar and Pomeau, 1997), and the ordered wrinkling of a buckled cylinders is similar to the well-known developable Yoshimura pattern in foldable tubes (Seffen and Stott, 2014). New corrugated structures made from developable strips connected together are one type of "morphing" structure, which combine highly directional compliance and stiffness for achieving large changes in shape whilst preserving structural integrity (Seffen, 2012); simple shells "growing" out of plane under imposed, so-called inelastic strains, must buckle into a variety of developable mode shapes for growth to proceed efficiently (Seffen and Maurini, 2013).

In the Appendix at the end of paper, the main details of Inextensional Theory and pertinent examples are repeated from Mansfield (1989) for completeness. In the following section, the relevant kinematical assumptions and definitions are outlined ahead of processing the geometrical data from experiments in Section 3. Two types of experiment are carried out on the same theoretical examples from the Appendix. The first are physical experiments on a triangular plate loaded by a force applied to its tip. The deformed state is accurately recorded using a laser-scanning camera, and the process of obtaining generator information from the measured displacements is carefully described. The method is effective but the maximum displacements that can be wrought are limited for reasons described, although we far exceed Manfield's nominal limit of a single thickness. Therefore, our second "experimental" study is finite element analysis, which allows us to circumvent some of the practical issues faced before and to test the robustness of the assumptions of Inextensional Theory in earnest. Most notably, the induced deformation can be much larger and geometrically non-linear, and we can apply end-wise moments. We therefore consider swept plates with a broad free edge to which end moments can be applied, as well as the previous tip-loaded triangular plates. All results are compared in Section 4, before finishing with a discussion and conclusions.

2. Kinematics

Following Mansfield, Fig. 1 shows the planform of a thin, cantilever plate of general outline, rigidly built-in along one straight edge. The absent loading is applied normal to the plate, and the deformed surface is taken to be developable, where straight-line generators can be drawn through every point on the surface. By definition, there is no twist and curvature along a generator, only curving across and normal to it. Elemental slices of deformed plate are bounded by adjacent generators, which do not have to be parallel, so each slice deforms into a element lying on part of a hypothetical conical surface. The curvature of this element varies inversely with distance, η, along the generator, where the origin of coordinate is taken to be the conical vertex; because the curvature at this point is infinitely large, the vertex must lie outside the planform, as shown. The vertices of successive generators form a locus known as the generatrix, and their inclination is measured by the angle, α, with respect to some arbitrary datum line with ordinate, X. Crucially, all geometrical parameters are specified with respect to the original flat plane even though parts of the deformed plate may lie well above or below it: without this specification, the kinematics are simply unwieldy and tractable solutions for the layout of generators expressed via (α, X) are not forthcoming. As we shall show, this does not undermine the accuracy of results, even for relatively large displacements. This specification also dictates that the layout of generators remains fixed and *independent* of the loading magnitude, provided linear elasticity prevails. As a corollary, we only need to perform a single set of measurements on a deformed, thin plate without measuring the load: this reduces the number of tests to be performed as well as simplifying the practical set-up.

In these tests, we accurately measure the displaced shape of plate in Cartesian space and then compute the changes in plate curvature: in finite element analysis, these curvatures are directly available. In order to compare directly to solutions from Inextensional Theory, these curvatures are converted into generators using a Mohr's circle of twisting curvature versus ordinary curvature (Calladine, 1983). For every point on a developable surface, the Mohr's circle passes through its own origin, giving way to one non-zero principal curvature—the local conical curvature, κ_1. However, the asymptotic nature of Inextensional Theory suggests that membrane strains everywhere may be very small and not absolutely zero. Of course, these could be measured directly (although not easily) but we note from Gauss that only their particular spatial variation within the surface affects the developable assumption. In other words, if there is *Gaussian*, *i.e.* double curvature, then membrane strains are significantly present. Commensurately, we assume that the Mohr's circle has a small second principal curvature, κ_2, and we define a corresponding measure of the degree of membranal stretching—the stretching ratio, SR—such that

$$SR = \left|\frac{\kappa_2}{\kappa_1}\right| \tag{1}$$

which is calculated throughout the plate.

It turns out that this ratio is always a small number, with only moderate increases in value close to the edges of plate where the assumed conical shape does not comply with the requirements of the free-edge boundary condition. A boundary layer forms in practice to facilitate this requirement, where the original proponent, Basset (1890), estimates the width of layer to be "`comparable with the thickness [of plate]`"; much later, Mansfield (1989) carries out a formal calculation and shows its width is of the order of $\sqrt{t\kappa}$, where t is the thickness and κ the change in curvature of the plate. Since the ratio is very small elsewhere, it becomes appropriate to define an acceptable threshold below which membrane effects may be assumed to be negligible. We can examine the performance of points "lying" above or below this threshold, in order to appreciate the prevalence of inextensionality and, when we vary the threshold, we can observe how the character of this distribution fares. For example, when the threshold is lowered, more data points are classified as being extensional, and they grow in number, primarily, from the boundary of the plate inwards. However, extra points in the middle of the plate away from any edges also become classified as extensional even though conical displacements are clearly evident there when the shape of plate is inspected visually. The reason is because the threshold now equates with the level of noise inherent during numerical processing of the data. After trial and error, we set the threshold to be 0.02,

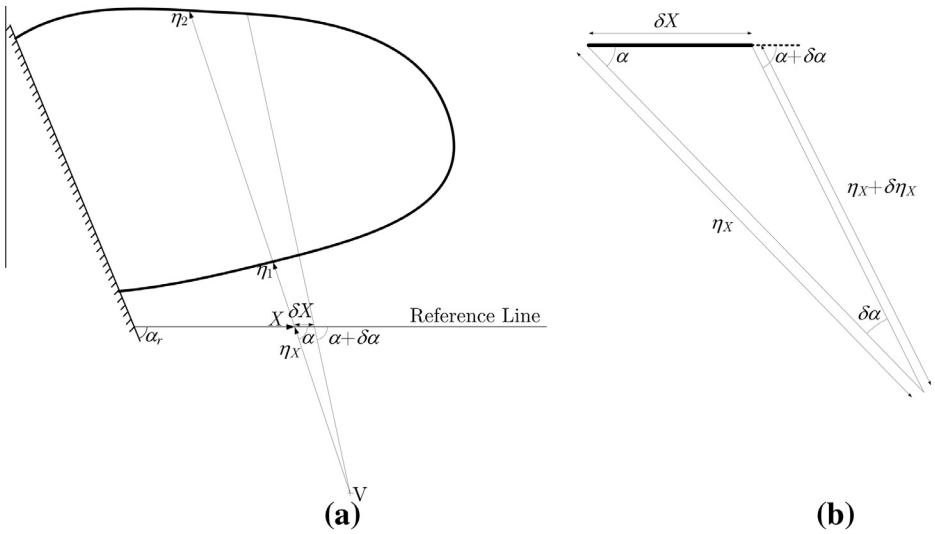

Fig. 1. (a) A general plate clamped along one end at an angle α_r to a reference line. The loads, which are not shown, are applied transversely, causing the plate to deform normal to the plane of the page. The deformation everywhere is assumed to be developable under the assumption of inextensionality of the plate middle surface, which manifests as a conical displacement field of inclined generators within the original planform. A typical generator is shown at a distance X along a reference datum line, inclined at an angle α to it. The distance between the vertex, V, and X is η_X, while the respective distances of V to the closer and further plate boundaries are η_1 and η_2. In addition, the adjacent generator is also shown at an incremental distance δX, inclined at an angle $\alpha+\delta\alpha$. (b) An infinitesimal element of the reference line at X, with two adjacent generators, which is used to calculate the continuity condition in the Appendix.

which is small enough for us to assert that membranal effects can be neglected for points complying with this value; but large enough to avoid giving false readings of significant membranal action. This may seem somewhat arbitrary, but the method is clearly validated when we transform the principal curvatures into generator data before comparing to theoretical predictions, where the correlation turns out to be very close indeed.

3. Testing methods

3.1. Experimental analysis

The experimental set-up is shown in Fig. 2. The triangular plate is made of flexible High Impact Polystyrene (HIPS) of thickness 0.25 mm and various planform sizes, as recorded in Table 1. Each plate hangs vertically in a holding rig to eliminate self-weight loading normal to the plate, and a tensioned string attached to the tip provides a transverse point force, which is maintained by an adjustable weight and pulley system. The height of the pulley can be varied so that the string always remains horizontal for a given tip-displacement, preventing the formation of in-plane forces everywhere else. As noted before, we do not need to measure the force in the string as we are only concerned with the geometry of deformation. To this end, we specify a tip deflection of several millimetres, well above the nominal level of a single thickness assumed by Mansfield for developable deformations, but low enough to ensure that the plan-view of the plate is not distorted perceptibly for reasons described next.

A three-dimensional (3D) image of the deformed shell is obtained using a *Vialux zSnapper*® 3D Scanner (htm, 2013). This scanning system consists of a camera for capturing images of the plate, and a projector which flashes light of various patterns and frequency onto the surface. The images are fed into the commercial software package accompanying the camera, which leads to a three-dimensional image of the surface of interest, in particular, the image data are rendered as a "point-cloud" in cartesian coordinates, uniformly spaced with respect to the original vertical plane and containing up to 300000 points. At the manufacturer's recommended maximum distance of 1.1 m from the specimen, the coordinate resolution of the camera is 125 μm, which reduces when the camera is brought nearer at the expense of a smaller field of view. Point-cloud data are obtained when the plate is load-free and then loaded and, by subtracting one set from the other, we begin to establish an absolute measure of the deformed shape and

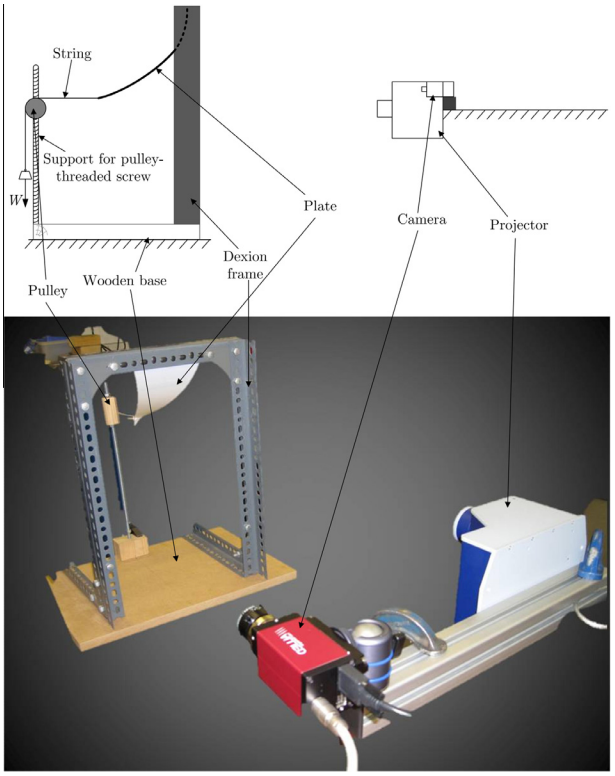

Fig. 2. Schematic and picture (background removed) of the experimental set-up for loading and recording the deformation of triangular cantilever plates. The camera and projector perform together as a three-dimensional scanner, which captures the deformed shape as a finely resolved point-cloud in Cartesian space. Information about the plate curvatures is then extracted from these coordinates, in order to compare to other predictions. Note that the tip deflection has been exaggerated in both views: the experimental values are much less so that the planform of plate is approximately conserved in the field of view but large enough so that the plate deforms into a developable surface.

Table 1
The geometric parameters defined in Fig. 4 of the three tested examples of triangular plate. The unit of the length, L, is millimetres for the experiments but is dimensionless for the finite-element analysis (all other properties being conserved).

L (mm)	ϕ (°)	α_r (°)
255	30	90
100	19	120
100	30	70

displacements. We cannot track the performance of points in the plate directly because the method simply records where the initial and deformed plates cut across the laser lines. Thus, we ensure that the initial plate is set normal to the projected direction so that normal displacements are, indeed, transverse displacements of the plate; and we also restrict the maximal displacements to around one-tenth of the length of plate so that points in the plate are moving purely at right angles to the original plane; under larger displacements there will be in-plane movement of points as well as transversal, and we lose track of the performance of points fixed in the plate. Note that for the largest plate, this equates to an absolute tip displacement of 25 mm, some 100 times its thickness.

The principal curvatures, κ_1 and κ_2, and their directions, are found by considering a point of interest, P, in the point-cloud, as shown in Fig. 3(a), where a local coordinate system, (x,y), specifies the intrinsic location of P within the original planform with respect to a known origin O. Except for boundary points, P has eight nearest, symmetrically-placed neighbours, where triplets of points lie along one of four directions separated by 45°, see Fig. 3(b). The spatial curvature along each direction is found from fitting a circular arc exactly along each set of three points, giving four ordinates on a Mohr's circle of curvature. Because the directions between triplet lines are known, only three of these curvatures are required to specify the centre and radius of the Mohr's circle such that it passes through the origin of axes; the values of twisting curvatures automatically follow. This would preordain the expectation of a developable shape, so we use the fourth ordinate rather than the origin to complete the Mohr's circle, Fig. 3(c), giving a faithful account of the deformed surface, which may not pass through the origin. From this, κ_1 and κ_2, are calculated and their principal direction, denoted by θ_g, relative to x and y is found. The stretching ratio, Eq. (1), is calculated and compared to the threshold of 0.02: if the ratio is smaller, θ_g is taken to be the local direction of the generator and κ_1 is declared to be the conical curvature, otherwise points are removed from the data set. Once θ_g is collated throughout the plate, it is then transformed into the global coordinates (α,X) from theory by projecting the generator until it intersects the datum line, X, whose origin, O_X, and orientation with respect to the plate match those used in the theoretical solution, see Fig. 3(d). Note that points which lie on the boundary have five neighbours but there is only one triplet of points through P: the Mohr's circle cannot be constructed fully, and so these points are removed from consideration, and justifiably so because of the high density of points in the bulk of plate.

3.2. Finite-element analysis

A finite-element analysis is performed using the commercially available software ABAQUS (Hibbitt et al., 2011). All plates are assumed to be made of a general linear-elastic material of Young's modulus, $E = 10^6$ units and Poisson's ratio, $\nu = 0.3$, and all have a plate thickness, t, equal to 0.1 units. These are nominal values which do not affect the expected generator layout, all other features being identical to experiments such as the planform shape, boundary conditions and loading type. All plates are effectively clamped at the root by constraining all nodes there in both displacement and rotation. Quadrilateral S4R shell elements of four nodes are used because they allow for large rotations under small strains, and the mesh is generated automatically by the software by specifying an approximate size for each quadrilateral element. All elements are also capable of in-plane extension and out-of-plane bending, so that the extent of inextensional behaviour can be readily checked. For cases of triangular plates, the loading at the tip is controlled by specifying an increasing displacement normal to the original flat plane, as in the experiment, and not as a "follower"-type load. For cases of swept plates, the loading is controlled by increasing the rotation of the free edge. In all, a geometrically non-linear analysis is performed to enable accurate large displacements, and this is applied in increments up to a nominal displacement limit using implicit, time-stepping methods based on a Simpson integration method (Riley et al., 2006).

The curvatures, κ_x and κ_y, and twisting curvature, κ_{xy}, are written at every node in a local (x,y) coordinate system. Using a Mohr's circle again, the principal curvatures, κ_1 and κ_2, are calculated, and their direction, θ_g, relative to (x,y) are obtained by the simple relationship, $\tan 2\theta_g = 2\kappa_{xy}/(\kappa_{xx} - \kappa_{yy})$. As with the physical data, the smaller principal curvature is never zero, so we employ the same process for identifying and discarding extensional nodes when the value of Eq. 1 exceeds 0.02. Because it is easy to arrange during the original meshing procedure, we set x to be aligned with the global datum line, X, and θ_g is equal to α from theory: the generator is then projected to where it meets X, in order to find each generator's ordinate.

4. Results

4.1. Example I: triangular plate

The schematic layout of an undeformed triangular plate is shown in Fig. 4(a). It is characterised by the tip vertex angle, ϕ, the inclination of the root clamp to the lower edge, α_r, and the length, L, of the lower edge. The origin of the (x,y) coordinate system is located at the tip with x and hence, X, moving along the lower edge. Fig. 4(b) includes extra detail used for the solution in the Appendix, namely, the auxiliary coordinate, β, and it shows that the tip generator at $X = 0$ is always taken to be perpendicular to the tip bisector. The three planform geometries in Table 1 describe square, obtuse and acute root angles, respectively, and the finite element analysis uses a mesh size where elements have a side-length of approximately 5 mm. The first plate is shown in Fig. 5(a) covered with its mesh, and in Fig. 5(b), the resulting deformed shape to indicate the degree of displacement: the point-cloud data from the 3-D scanning method has been illustrated in Fig. 3(a).

For this case, Fig. 6 compares the variation of generator angle, α, with dimensionless position, X/L, between theory (red), finite element analysis (blue points) and physical experiments (black dots). All available nodes in the finite element mesh are represented except for those that lie above the stretching ratio threshold, which are mostly located near the free edges. The data points shown follow the theoretical trends very well although there is some scattering in the points along the general path. This is due to the natural level of sensitivity inherent to the processing of geometrical data, which tends to be exacerbated when the generators are nearly parallel to each other. But we note that the range of scatter and the levels of discrepancy between the trends are incredibly small, being less than one degree. In the region between the tip and $X/L \approx 0.3$, there are missing data points, not because of significant membranal action there, but as an artefact of the small bending moments that form along nearby generators. These moments are

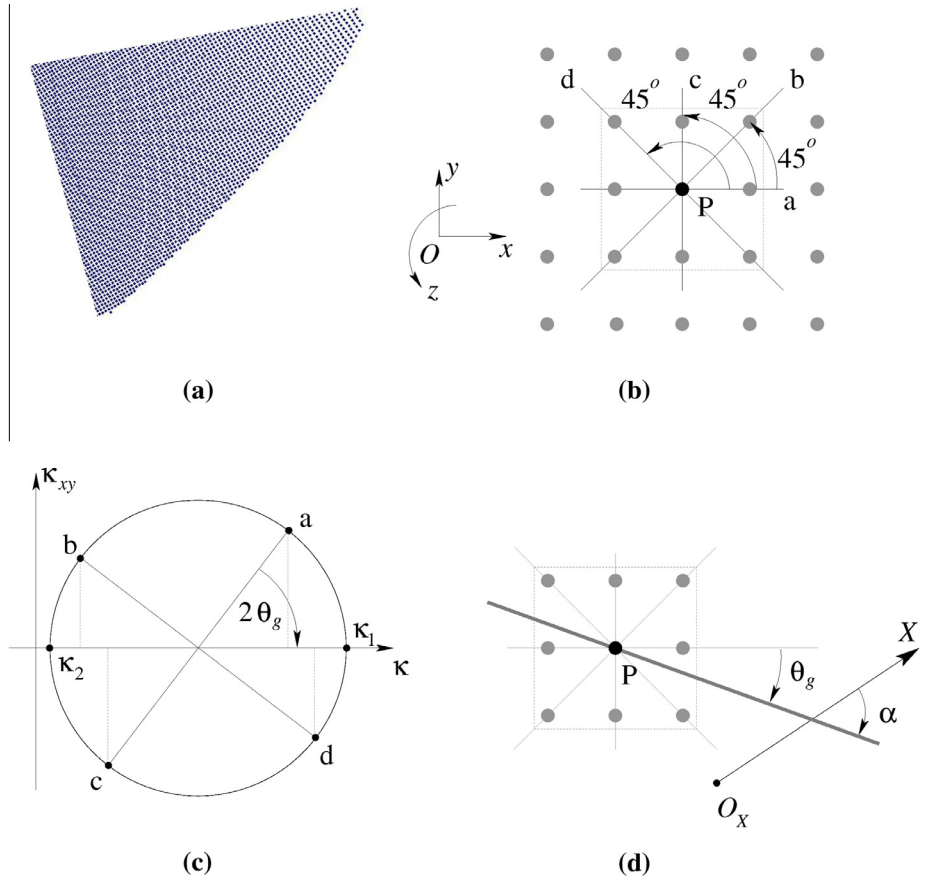

Fig. 3. Processing the point-cloud data obtained from the experiment in Fig. 2. (a) A typical point cloud of the first triangular plate from Table 1 in its deformed state: the right-hand tip is loaded and the left-hand edge is clamped. (b) A schematic sample of the point cloud around a point of interest, P. The camera produces a uniformly-spaced mesh of points where the local planform coordinates are (x,y), with transverse displacements in the z-direction normal to the plane of page. Four directions, a, b, c and d are drawn through each triplet of points with P in the middle, and the spatial curvature along each of them is calculated by fitting circular arcs exactly: the density of points is high enough so that the rate of change of curvature is negligible across each triplet. (c) A Mohr's circle of twisting curvature, κ_{xy} versus curvature, κ is constructed by fitting the best circle to the ordinate values of the curvatures found along *a* to *d*. From this, the principal curvatures, κ_1 and κ_2 and their inclination, θ_g, are calculated. The latter is the generator direction at P provided $\kappa_1 \gg \kappa_2$, subject to the stretching ratio in Eq. (1). (d) The generator (grey) is projected onto a global datum line, X, given by theory, so that the corresponding global generator angle, α can be found for each point. The origin, O_X, of X is also specified by theory, depending on the problem, and may be different to the local coordinate system.

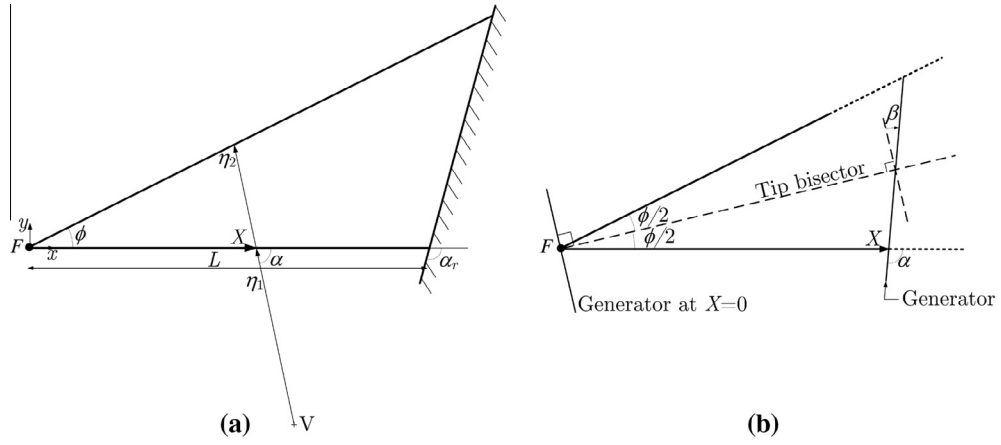

Fig. 4. (a) Geometrical layout of a tip-loaded triangular cantilever plate. The bottom edge, or boundary, is always parallel to the global x-axis and has length, L. At its root, the plate is clamped along another edge at angle, α_r. The angle subtended at the tip is ϕ, where the transverse force is F. A given generator at a distance X (parallel to x) from the tip makes an angle α to the bottom boundary: the distances from the vertex of the conical element, V, to the two boundaries are η_1 and η_2 as shown. (b) Tip region of the triangular plate showing the generator at $X = 0$, and a given generator at X illustrating the definition of the angle $\beta = \alpha - (\pi/2 - \phi/2)$, measured from the perpendicular to the tip bisector. This definition is formulated so that at the tip $\beta = 0$, which marginally simplifies the analysis presented in the Appendix.

linearly dependent on the lever arm of the applied force where, close to the tip, they are small, and consequently the conical curvature is small. This predisposes a small Mohr's circle during data processing, which increases the sensitivity of Eq. (1) to the lowest principal curvature, κ_2, and lowers the threshold below which membranal effects can be considered negligible. We can reduce

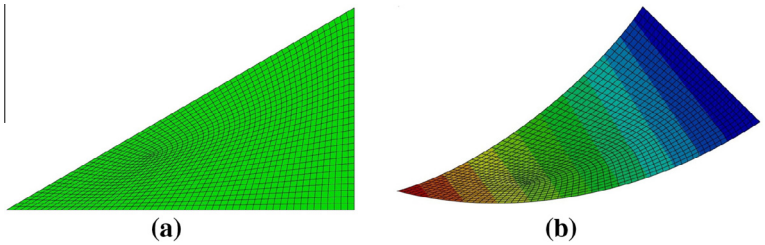

Fig. 5. (a) Finite-element model of the first undeformed triangular plate, overlaid by its mesh. (b) Deformed plate after finite element analysis in perspective view with contours of constant rotation highlighted.

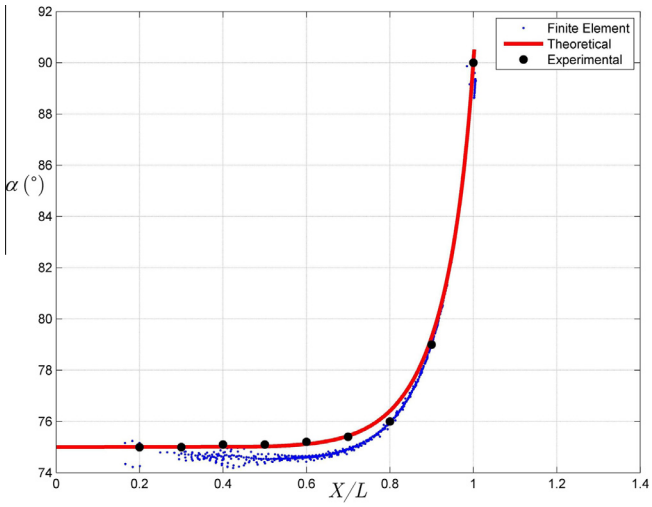

Fig. 6. Variation of generator angle, α, *vs* non-dimensionalised length, X/L, for the first triangular plate in Table 1: theory (Appendix: red solid line), finite-element analysis (blue points) and physical experiments (black dots). Each node's performance from the finite element data is included provided its stretching ratio, Eq. (1), does not exceed 0.02: if so, then points are excluded from the data set, and this occurs close to the tip and along both edges of plate. The corresponding physical experimental data have been sequenced at fixed intervals of X/L, for the sake of compactness, to obtain the corresponding (averaged) value of α. (For interpretation of the references to colour in this figure legend, the reader is referred to the web version of this article.)

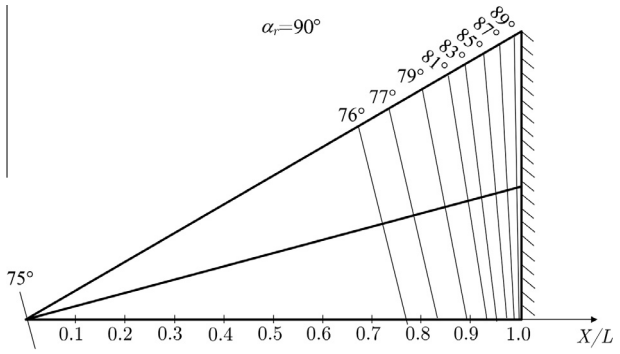

Fig. 7. Generator distribution along the plate using the results from the physical experiments. The tip generator angle of 75° is taken from theory and plotted for reference: each of the other generators has been sequenced from the point-cloud data at fixed intervals of α to obtain the corresponding value of X/L from which the generator lines can be plotted and drawn.

the threshold so that points in this region remain in the data set but at the expense of removing more points near the edges; but we choose not to because we understand why. On the other hand, all of the data points from the physical experiments cannot be plotted in the same way because their density is so high—recall that up to 300,000 points can be tracked by the camera. Instead, their data for α are averaged within fixed intervals of X/L, resulting in a reduced, regularly spaced set of points: these follow the theoretical line almost exactly.

When X increases, theory suggests that successive generators are almost parallel for most of the way along the plate, being initially perpendicular to the tip bisector, before they turn sharply close to the root. This is matched by both the finite elements and physical experiments, and is more clearly evinced when the generator distribution via experimental data is superposed onto the original planform in Fig. 7. In the remaining two cases in Fig. 8, both the experiments and finite element analysis are almost indistinguishable from the theoretical predictions. For $\alpha_r = 120^\circ$, α turns more sharply moving towards the root with very little scatter in the results. For $\alpha_r = 70^\circ$, the generators rotate in the opposite sense to before, with α decreasing towards the root over a smaller range compared to the other two cases. Its conical vertices lie above the plate in plan-view, and so the reference edge for X is the top boundary because convention assumes it is the closest; but α is measured with respect to the bottom boundary, also by convention, hence, these angles are shown there instead. Overall, the trends and the correlation between results and theory are exceptionally close, which seems to vindicate the effectiveness of Inextensional Theory.

4.2. Example II: swept plate

The schematic layout is defined in Fig. 9 by the root angle α_r, transverse width w, and length L, along the plate centre, which is chosen to be $5w$: the length of plate does not have to be specified in theory since the plate could be clamped along any given generator without altering the layout of generators ahead. A length needs to be specified in the finite element analysis, and $5w$ is found to be large enough so that generators become parallel and aligned to the tip well before. This length is set to a nominal value of 100 units, and the mesh-size is chosen to have a side-length of approximately 2 units. Displacement control is again specified with the free edge undergoing a unit radian rotation, and two values of α_r are chosen, 45° and 60°, with the first mesh shown in Fig. 10 before and after deformation.

The analytical solution is given in the Appendix, and is compared with the finite element data for both root angles in Fig. 11. The correlations are very good although some scatter in the data points is evident close to each plate tip, where the generators are nearly parallel—as previously observed in the triangular cases. Both sets of generators turn sharply towards the root, and the general trends in α are again exceptionally close, deviating by no more than one degree from one another.

5. Discussion and conclusions

We have revisited Inextensional Theory for computing the deformed and developable shape of thin plates. Some limited

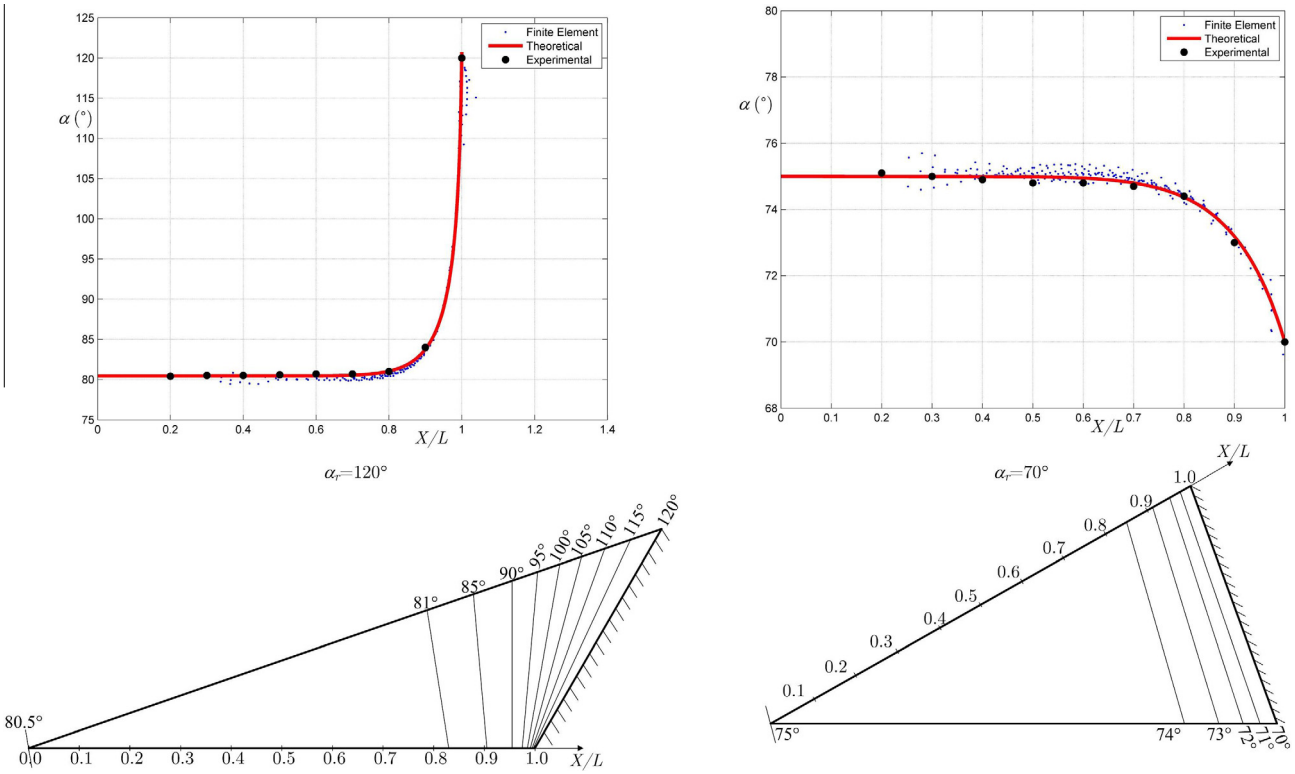

Fig. 8. Variation of generator angle, α, *vs* non-dimensionalised length, X/L, for the two remaining triangular plates in Table 1: theory (Appendix: red solid line), finite-element analysis (blue points) and physical experiments (black dots: sequenced as per Fig. 6). The stretching ratio threshold, Eq. (1), is equal to 0.02. The generators are overlaid in the bottom views for additional clarity. (For interpretation of the references to colour in this figure legend, the reader is referred to the web version of this article.)

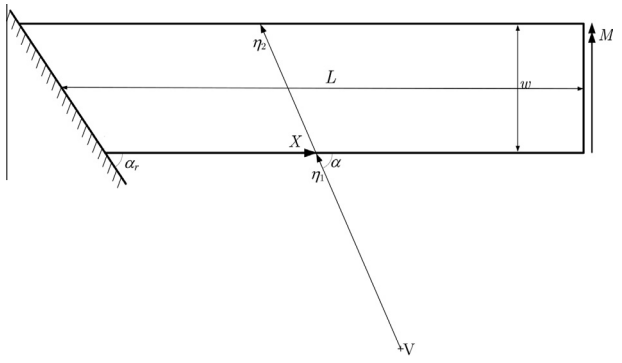

Fig. 9. Swept cantilever plate of width w and length, L, at mid-width with $L \gg w$. It is clamped at its root end at angle α_r to the bottom edge of plate, and a moment, M, is applied to the free end. A typical generator is shown at a distance X from the root end along the reference line, which coincides with the bottom edge.

experimental validation has been conducted before, but there have been no experiments dedicated to capturing the entire shape of plate, which Inextensional Theory elegantly renders as a layout of conical generators. We first measured the deformed shape of plate using a highly accurate, laser-scanning camera, which produces a point-cloud of data in three-dimensional Cartesian space. We then computed the changes in plate curvatures along local directions; we fitted a Mohr's circle to the data points, and then extracted the principal curvatures. We then calculated the ratio of principal curvatures, in order to define a simple measure of possible membranal effects. By setting an acceptable upper limit on this ratio, we were able to identify points in the plate deforming practically inextensionally. For these points, we then transformed the principal curvatures into generator curvature and orientation, in order to compare directly with theoretical solutions. We also performed a number of finite element analysis for a comparison. The correlation between all methods was excellent, and this gives confidence to Inextensional Theory, particularly with renewed interest in problems involving large developable deformations of thin plates and shells: in that connection, it is important to be clear again about the primary assumptions.

The method ascribes a layout of generators with respect to the original flat planform of plate even though ultimately displacements normal to the plate can several thicknesses—and more, as we have shown. Because displacements are ancillary to the method, it circumvents the inherent difficulties with prescribing geometrical non-linearity from the outset; a parallel example is pure bending of rod by end moments into a circular arc, whose deformed shape is more simply rendered in terms of the curvature

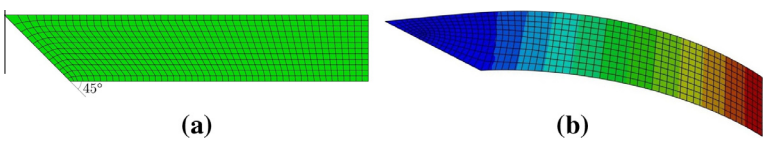

Fig. 10. (a) Swept plate with a root angle of 45° overlaid with its mesh set-up in ABAQUS. (b) Deformed plate under end-wise moment after finite-element analysis, in perspective view with contours of constant rotation. The final rotation of the free end is one radian.

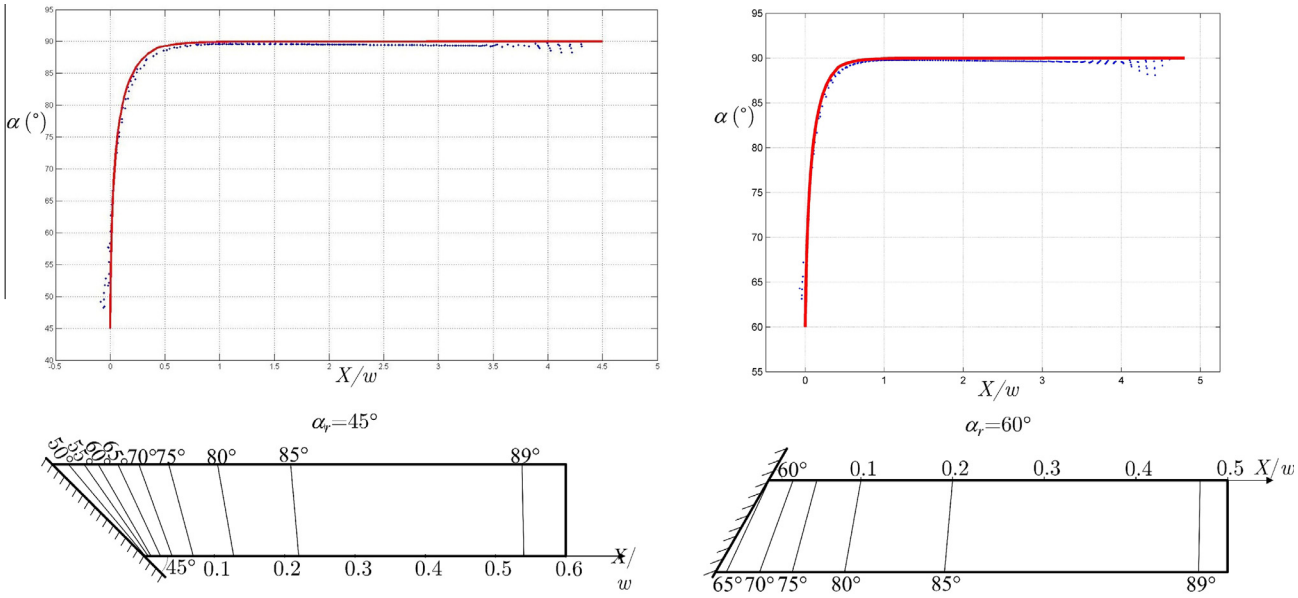

Fig. 11. Variation of generator angle, α, *vs* non-dimensionalised length, X/w, for swept plates having root angles of 45° and 60° and loaded by end-wise moments: theory (Appendix: red solid line) and finite-element analysis (blue points). The stretching ratio threshold is 0.02, Eq. (1), and the generators are overlaid in the bottom views. (For interpretation of the references to colour in this figure legend, the reader is referred to the web version of this article.)

change rather than the displacements which follow. The number of generators is not defined by the method: for solutions of $\alpha(X)$ in closed form, there is a continuous variation and infinite number; by their very nature, numerical solutions have a finite number dictated by the chosen step interval. Overall displacements can be found from the generator curvatures by integration: the more finely-spaced the generators, the more accurate the final displacements relative to the continuously-variable case. The same is true of the analogous Tension Field Theory in which the number of wrinkling "tension" rays in a thin sheet is not formally defined but their direction is. The priority in this case is not finding the overall distortions of the sheet, rather the properties of individual wrinkles that form as a finite number, in practice, which is determined by other, more elaborate studies: in this sense, the aims of the two Theories diverge. If the true plate displacements here are very large, then the applied loading changes position significantly during deformation, which ought to alter the internal bending moment distribution and ultimately the effectiveness of the Inextensional Theory. We recognised earlier that this may present problems for interpreting experimental data; but where this was not an issue during computational studies, the presence of very large displacements does not appear to undermine the quality of predictions.

As Mansfield attests (Mansfield and Kleeman, 1955), the size of plate does not affect the generator layout, nor does the choice of material provided it behaves in a linear elastic fashion. The shape of layout is, in essence, a statement of the equilibrium performance of the plate under loading; only the boundary conditions, the shape of planform and the *type* of loading have influences. Once these have been established, the layout is fixed; and because we are only interested in verifying layouts here, the loading magnitude and material units are inconsequential. The overall stiffness of plate, however, depends on all parameters, and thus any experimental verification requires a sensible choice so that final displacements are beyond being shallow. Curiously, Inextensional Theory predicts a linear overall stiffness despite relatively large displacements, which precludes the principle of superposition—in the context of adding together the effects of different types of load. The reason for linearity is because the bending moments are written in terms of the original flat plate for solution expedience; and Mansfield's original experiments in which he measures the force–displacement response, confirm matters (Mansfield and Kleeman, 1955).

We have not challenged the underlying premise of Inextensional Theory nor attempted to reconfigure its presentation. We cannot conclude, however, without mentioning the role of a possible broader principle. Cerda and Mahadevan (2005) show that the governing equation of deformation for Euler's famous *Elastica* rod applies to certain inextensional deformations of a cylinder and a cone: they derive equivalent governing equations in terms of the principal curvature of deformation in both cases, and then propose that equivalent problems in higher-order geometrical space can be classified as general *Elastica* solutions; if the same is true of Inextensional Theory, then the generalised deformation response of the plate is also part of the *Elastica* family. The point seems obvious but is only valid if we can verify that the plate deformation lies within the class of *Elastica* solutions. The comparative choice is the conical curvature, which is not directly output but is fairly trivial to calculate in terms of the generator angle using Eqs. (2) and (3) in the Appendix. The availability of closed-form solutions for α is, however, very limited, and those presented here are implicit expressions: thus, the curvature variation cannot be checked analytically on the whole, rather, the process has to be a numerical undertaking. This seems to us to be an interesting, and substantive, point to pursue in further work.

Acknowledgements

VRS was supported by a PhD studentship from the Engineering and Physical Sciences Research Council (EPSRC) of the United Kingdom. The thoughtful and supportive comments of two anonymous referees were gratefully received and implemented.

Appendix: general framework

The following framework and worked examples are taken from Mansfield (1989) but written in our style.

5.1 Governing equations

Fig. 1(a) shows an homogenous plate of constant thickness clamped along one edge at an angle, α_r, to a reference line. Also shown are two arbitrary, adjacent generators, which corresponds to an elemental slice deforming in a conical manner in accordance with the surface being developable under some transverse loading (not shown). Three conical parameters are required to completely specify the curvature along a generator: the inclination, α, of the generator measured from a reference line; the distance, η, between the vertex, V, of the conical element and a general point; and a size parameter of the conical section, c, such that the non-zero principal curvature at any point along the generator is given by

$$\kappa_\alpha = \frac{c}{\eta} \tag{2}$$

The position of the generator is represented by the distance X, where it intersects the reference line. Furthermore, the respective distances between the vertex and the intersection of the generator with the reference line, nearer and further plate boundaries are η_X, η_1 and η_2 (all dependent by geometry), respectively. The three independent variables, α, η_1 and c, are determined by the enforcement of three conditions as follows.

Continuity and Smoothness

For the deformed surface to be continuous and smooth, adjacent generators must share the same vertex, as illustrated in Fig. 1. Consider two adjacent generators separated by an infinitesimal distance δX along the reference line, with incremental inclination angle $\delta\alpha$, as shown in an expanded view of the reference line in Fig. 1(b). By using the sine rule and observing the limit as δX and $\delta\alpha$ both tend towards zero, noting that α is measured in radians, produces

$$\frac{d\alpha}{dX} = \frac{\sin\alpha}{\eta_X} \tag{3}$$

In the examples considered in this paper, the edge of the plate nearer to the vertex is straight and is used as the reference line. Therefore, $\eta_X = \eta_1$ and hence, the continuity equation can be written as

$$\frac{d\alpha}{dX} = \frac{\sin\alpha}{\eta_1} \tag{4}$$

which must hold for a smooth, continuous distribution of generators.

Equilibrium and Hooke's Law

The magnitude of the moment per unit length about the generator is dependent on the applied loading. The corresponding curvature is κ_α whilst the curvature perpendicular (along the generator) and twisting curvature are both assumed to zero. From the generalised Hooke's law for bending of an element of plate, (Calladine, 1983), where D is the flexural rigidity, then

$$m_\alpha = D\kappa_\alpha = \frac{Dc}{\eta} \tag{5}$$

using the definition of κ_α in Eq. (2). Integrating this equation over the entire length of the generator between the boundaries of the plate gives

$$M_\alpha = \int_{\eta_1}^{\eta_2} m_\alpha d\eta = \int_{\eta_1}^{\eta_2} \frac{Dc}{\eta} d\eta = Dc\ln\left(\frac{\eta_2}{\eta_1}\right) \tag{6}$$

where M_α is the total moment along the generator, c is constant along the generator, and D is assumed constant over the entire plate. The total moment along each generator is found from overall equilibrium considerations with the applied loading, and η_2/η_1 is determined from geometry.

Strain Energy

Inextensional Theory assumes that a generator is present through every point on the surface, effectively constraining the curvature and twist in this direction to be zero. This is tantamount to introducing a theoretical constraint to deformation which, if not in its true direction, would result in a smaller value of strain energy than the corresponding true energy (Southwell, 1941). Thus, the true directions of the generators (constraints) correspond to maximum strain energy stored in the plate. In general, the total strain energy, U, is (Calladine, 1983)

$$U = \frac{1}{2}\int_\alpha \int_{\eta_1}^{\eta_2} m_\alpha \kappa_\alpha \eta d\eta d\alpha = \frac{1}{2}\int_\alpha M_\alpha c d\alpha \tag{7}$$

since $\kappa_\alpha\eta = c$. Eliminating c using Eq. (6) results in:

$$U = \frac{1}{2}\int_\alpha \frac{M_\alpha^2}{D\ln(\eta_2/\eta_1)} d\alpha \equiv \frac{1}{2}\int_\alpha F_1 d\alpha \Rightarrow F_1 = \frac{M_\alpha^2}{D\ln(\eta_2/\eta_1)} \tag{8}$$

Or, expressing the integral in terms of X

$$U = \frac{1}{2}\int_\alpha \frac{M_\alpha^2}{D\ln(\eta_2/\eta_1)} \frac{d\alpha}{dX} dX \equiv \frac{1}{2}\int_\alpha F_2 dX \Rightarrow F_2 = \frac{\alpha' M_\alpha^2}{D\ln(\eta_2/\eta_1)} \tag{9}$$

where $\alpha' = d\alpha/dX$. The strain energy has been expressed in two different ways: the integrand F_1, has α as the independent variable and X as the dependent variable, and *vice versa* for F_2. Though both formulations are equivalent, one may be significantly easier to maximise than the other. From the calculus of variations, (Riley et al., 2006), the maximum value of U occurs when the variation of the generators satisfy the Euler–Lagrange equation given in two forms for the above cases

$$\frac{\partial F_1}{\partial X} - \frac{d}{d\alpha}\left(\frac{\partial F_1}{\partial X'}\right) = 0 \text{ or } \frac{\partial F_2}{\partial \alpha} - \frac{d}{dX}\left(\frac{\partial F_2}{\partial \alpha'}\right) = 0 \tag{10}$$

which govern the relationship between α and X. The resulting equation is subject to the boundary condition $\alpha = \alpha_r$ at $X = 0$, since the curvature along the root (generator) must be zero.

5.2 Theory: triangular plate

The schematic triangular planform is given in Fig. 4. The lower edge is assumed to be horizontal in view, and X defines a distance along this reference boundary. At the tip, the generator must either be perpendicular or parallel to the bisector of the tip angle by symmetry since St. Venant's principle dictates that the root has no effect on the behaviour here. However, in order to maximise the bending strain energy locally, the generator must be perpendicular to the bisector as shown in Fig. 4(b). It is more convenient to formulate the problem by measuring the angle from the perpendicular to the tip bisector, β, with $\beta = \alpha - (\pi - \phi)/2$, so that the boundary condition at the tip becomes $\beta = 0$ at $X = 0$.

By equilibrium, the moment, M_β, about the generator under a tip force, F, is given by $M_\beta = FX\cos(\beta - \phi/2)$ and, from geometry, the length of the generator between the boundaries is $\eta_2 - \eta_1 = X\sin\phi/\cos(\beta + \phi/2)$. But, $d\beta/dX = d\alpha/dX$, or compactly $\beta' = \alpha'$, so the continuity and smoothness equation, Eq. (4), can be expressed as

$$\eta_1 = \frac{\cos(\beta - \phi/2)}{\beta'} \tag{11}$$

and thus,

$$\frac{\eta_2}{\eta_1} = 1 + \frac{2X\beta' \sin\phi}{\cos\phi + \cos 2\beta} \equiv 1 + \mu \text{ with } \mu = \frac{2X\beta' \sin\phi}{\cos\phi + \cos 2\beta} \tag{12}$$

At the tip $X = 0$, so $\mu = 0$ from the above equation. The energy equation can be expressed in the form given in Eq. (9), with

$$F_2 = \frac{F^2 X^2 \beta' \cos^2(\beta - \phi/2)}{D \ln(1+\mu)} \tag{13}$$

When this expression is substituted into the Euler–Lagrange equation, Eq. (10), and recalling that $\alpha' = \beta'$, then

$$\frac{d\beta}{d\mu} = \frac{\cos\phi + \cos 2\beta}{(N \sin 2\beta)/\mu - 2Q \sin\phi} \tag{14}$$

where

$$N = \frac{4\mu^2(1+\mu)\ln(1+\mu)}{(2+\mu)\ln(1+\mu) - 2\mu} \tag{15}$$

$$\text{and } Q = \frac{(1+\mu)\ln(1+\mu)[\mu(2+\mu) - 2(1+\mu)\ln(1+\mu)]}{\mu[(2+\mu)\ln(1+\mu) - 2\mu]} \tag{16}$$

The governing equation, Eq. (14), relates β and μ, and is subject to the boundary condition $\beta = 0$ when $\mu = 0$. The most difficult part in the solution of this problem lies in dealing with the singularities at the loaded tip of the plate when Eq. (14) is integrated to obtain the relationship between β and μ. Once this relationship has been derived, the relationship between X, μ and β can be obtained by then integrating Eq. (12). The first integration has to be performed numerically, with the boundary condition at the tip, $\mu = \beta = 0$, subject to the boundary condition

$$\left.\frac{d\beta}{d\mu}\right|_0 = \frac{\sin\phi}{24}\left(1 + \sqrt{7 + 6\cot^2\frac{\phi}{2}}\right) = \gamma, \text{say} \tag{17}$$

The second integration follows after separating the variables in Eq. (12):

$$\int \frac{1}{X} dX = \int \frac{2\sin\phi}{\mu(\cos\phi + \cos 2\beta)} d\beta \Rightarrow \ln X = \int \frac{2\sin\phi}{\mu(\cos\phi + \cos 2\beta)} d\beta \tag{18}$$

Note however, that there is a singularity again at $\mu = 0$, and Mansfield (1955) suggests a clever method to get around this as follows, by introducing the function

$$T(\beta) = \frac{2\gamma \tan(\phi/2)}{\beta} - \frac{2\sin\phi}{\mu(\cos\phi + \cos 2\beta)} \tag{19}$$

The advantage of this function is that the first term is analytically integrable, the second term is the integrand in Eq. (18), and most importantly, $T(\beta)$ is finite at $\mu = \beta = 0$. Substituting Eq. (19) into Eq. (18) results in

$$\ln X = \int \frac{2\gamma \tan(\phi/2)}{\beta} - T(\beta) d\beta \Rightarrow X = C\beta^{2\gamma \tan(\phi/2)} \exp\left(-\int_0^\beta T(\beta) d\beta\right) \tag{20}$$

where C is the constant of integration, chosen to satisfy the boundary condition at the root, $\beta = \alpha_r - \pi/2 + \phi/2$ at $X = L$.

5.3 Theory: swept plate

A swept plate differs from the triangular plate by having parallel edges, leading to an easier analysis. As shown in Fig. 9, the plate end is loaded by a moment, M, and a generator at a distance X from the root along the lower edge of the plate is inclined at α. By equilibrium, the moment about a given generator is given by $M_\alpha = M \sin\alpha$ and, from geometry, the length of the generator between the boundaries can be written as $\eta_2 - \eta_1 = w \csc\alpha$. Combining these with the continuity and smoothness equation, Eq. (4):

$$\frac{\eta_2}{\eta_1} = 1 + w \csc^2\alpha \frac{d\alpha}{dX} \tag{21}$$

The integrand, F_1, of the energy equation, Eq. (8), is given by

$$F_1 = \frac{M^2 \sin^2\alpha}{D \ln\left[1 + (w\csc^2\alpha)/X'\right]} \tag{22}$$

and this is maximised using Eq. (10), yielding

$$X'^2\left(1 + \frac{w\csc^2\alpha}{X'}\right)\left[\ln\left(1 + \frac{w\csc^2\alpha}{X'}\right)\right]^2 = \text{ constant} \tag{23}$$

As X gets large, the generators become parallel to the applied moment, and so α converges to $\pi/2$ and X' tends towards infinity. The constant on the right hand side is found to be equal to w^2, and Eq. (23) can be re-written as

$$\left(\frac{X'}{w}\right)^2\left(1 + \frac{w\csc^2\alpha}{X'}\right)\left[\ln\left(1 + \frac{w\csc^2\alpha}{X'}\right)\right]^2 = 1 \tag{24}$$

subject to the boundary conditions $\alpha = \alpha_r$ when $X = 0$ (at the root). The variation of α with X can be found by numerically integrating Eq. (24).

References

Basset, A.B., 1890. On the extension and flexure of cylindrical and spherical thin elastic shells. Philos. Trans. R. Soc. London A 181, 433–480.

Ben Amar, M., Pomeau, Y., 1997. Crumpled paper. Proc. R. Soc. London Ser. A 453, 729–755.

Calladine, C.R., 1983. Theory of Shell Structures. Cambridge University Press.

Cerda, E., Mahadevan, L., 2005. Confined elastic developable surfaces: cylinders, cones and the elastica. Proc. R. Soc. London A 461, 671–700.

Giomi, L., Mahadevan, L., 2010. Statistical mechanics of developable ribbons. Phys. Rev. Lett. 104, paper 238104.

Hibbitt, D., Karlsson, B., Sorensen, P., 2011. ABAQUS Manual version 6.11, Dassault Systemes.

<www.vialux.de/HTML/enddscan.htm> 2013. Vialux.

Mansfield, E.H., 1955. The inextensional theory for thin flat plates. Q. J. Mech. Appl. Math. VIII (Pt. 3), 338–352.

Mansfield, E.H., 1989. Bending & Stretching of Plates. Cambridge University Press.

Mansfield, E.H., Kleeman, P.W., 1955. A large-deflexion theory for thin plates. Aircr. Eng. 27, 102–108.

Niven, W.D., 1890. The Scientific Papers of James Clerk Maxwell. Dover Publications, New York, 1, pp. 81–114.

Riley, K.F., Hobson, M.P., Bence, S.J., 2006. Mathematical Methods for Physics and Engineering. Cambridge University Press.

Seffen, K.A., 2012. Compliant shell mechanisms. Philos. Trans. R. Soc. London A 370, 2010–2026.

Seffen, K.A., Maurini, C., 2013. Growth and shape control of disks by bending and extension. J. Mech. Phys. Solids 61 (1), 190–204.

Seffen, K.A., Stott, S.V., 2014. Surface texturing through cylinder buckling. J. Appl. Mech. ASME 81 (1), paper 061001.

Southwell, R.V., 1941. An Introduction to the Theory of Elasticity for Engineers and Physicists. Oxford University Press.